BMC Cancer

RESEARCH Open Access

Development and validation of basement membrane-related signatures for predicting postoperative recurrence, tumor microenvironment and drug candidates in chordomas

Tianhao Zhang[1], Mingxuan Li[1], Xing Liu[2], Sida Zhao[1], Tianshun Ma[1], Yide Liu[1], Xijia Zhang[3], Qian Liu[1], Jiwei Bai[3] and Yazhuo Zhang[1,3,4,5*]

Abstract

Background Skull base chordoma is a rare and aggressive bone tumor with a poor prognosis. The basement membrane (BM) plays an pivotal role in tumor progression. However, the involvement of BM-related genes in assessing the prognosis and influencing the biological behavior of skull base chordomas remains unclear.

Methods Patients with skull base chordoma undergoing endoscopic endonasal surgery were included in the study (77 patients for bulk transcriptome sequencing and 6 patients for single-cell RNA sequencing). A BM-related genes signature was established and validated using bulk transcriptome data. Additionally, we investigated the oncogenic potential of a key BM-related gene in chordoma cells in vitro.

Results A prognostic signature consisting of five BM-related genes was identified through LASSO Cox regression analysis. The accuracy and reliability of this signature were validated by the validation cohort. Multivariate Cox analysis and a nomogram demonstrated that the risk score serves as an independent and reliable prognostic factor for skull base chordoma. Moreover, the BM-related gene signature was significantly associated with the immune microenvironment, immune checkpoint expression, and drug sensitivity. Single-cell RNA sequencing analysis revealed both the chordoma tumor cell and the fibroblast contributed to the overall BM signature. Finally, in vitro experiments demonstrated that the knockdown of ITGB3, the hub gene in the signature, inhibited the proliferation and migration of chordoma cells via the PI3K-Akt pathway.

Conclusion This study explored the critical role of BM-related genes in skull base chordoma, which affected postoperative recurrence and maligant behavior of chordoma via the PI3K-Akt signaling pathway.

Keywords Skull base Chordoma, Base membrane, Prognostic, Immune, Drug sensitivity, PI3K-Akt signaling pathway

*Correspondence:
Yazhuo Zhang
zyztxzz@126.com

Full list of author information is available at the end of the article

© The Author(s) 2025. **Open Access** This article is licensed under a Creative Commons Attribution-NonCommercial-NoDerivatives 4.0 International License, which permits any non-commercial use, sharing, distribution and reproduction in any medium or format, as long as you give appropriate credit to the original author(s) and the source, provide a link to the Creative Commons licence, and indicate if you modified the licensed material. You do not have permission under this licence to share adapted material derived from this article or parts of it. The images or other third party material in this article are included in the article's Creative Commons licence, unless indicated otherwise in a credit line to the material. If material is not included in the article's Creative Commons licence and your intended use is not permitted by statutory regulation or exceeds the permitted use, you will need to obtain permission directly from the copyright holder. To view a copy of this licence, visit http://creativecommons.org/licenses/by-nc-nd/4.0/.

Background

Chordoma is a rare and aggressive malignant tumor that arises from remnants of the notochord, primarily affecting the central axial bones, such as the clivus, spine, and sacrum [1, 2]. Currently, the mainstay of treatment for chordoma typically involves maximal surgical resection combined with localized proton radiation therapy [3]. However, the challenging anatomical location skull base chordomas complicates the feasibility of complete surgical excision. Although chordomas tend to exhibit slow growth, their biological behavior is highly destructive with a high recurrence rate [4]. Currently, the pathogenesis and clinical prognostic stratification system of chordoma is not well defined, and novel prognostic biomarkers and therapeutic targets are urgently needed.

The basement membrane (BM) is a thin, dense sheet of extracellular matrices widely distributed in metazoan tissues playing an important role in normal tissue development and function [5]. Core structural components of BM include laminins, collagen IV, nidogens, and the heparan sulfate proteoglycans perlecan and agrin, which participate in resisting mechanical stress, dictating tissue shape, and creating diffusion barriers [6, 7]. They also provide cues that direct cell polarity, differentiation, migration, and survival [8]. The variants of the above molecules underlie the development of various human diseases [9]. Particularly, the aberrant expression of BM-related genes is associated with tumor progression in multiple cancers [10–13]. Histologically, chordomas have extensive extracellular matrices between tumor cells, which may portend an unfavorable prognosis [14]. In the presence of cancer-associated fibroblasts (CAF), cancer cells could invade the BM in a metalloprotease-independent manner [15]. Recently, studies revealed the presence and oncogenic role of CAF in skull base chordoma [16], suggesting BM-related genes may participate in the progression of skull base chordoma. However, there are few studies on BM in chordoma.

This study aimed to investigate the role of BM-related genes in skull base chordoma. By analyzing the bulk transcriptomic data and the clinical information, we constructed a prognostic signature composed of five BM-related genes to predict recurrence-free survival (RFS) in chordoma patients. We also explored the association between the risk score and tumor immune and drug sensitivity in chordoma. Furthermore, one hub gene, ITGB3, was knocked down in two chordoma cell lines to investigate its biological function. In summary, this study assesses the prognostic value of BM-related genes in skull base chordoma, examines their biological roles, identifies potential therapeutic agents, and aims to improve the clinical outcomes for chordoma patients.

Methods

Patients and data collection

In total, 83 patients diagnosed with skull base chordoma and received endoscopic endonasal surgery at our hospital, were included in this study. We acquired the raw bulk transcriptome counts data of 77 skull base chordoma samples in batches and the normalized and log2 converted RNA-sequencing (RNA-seq) profiles TPM. The first batch of RNA-seq data, consisting of 48 cases, was used as the training cohort in this study, which was reported in our previous article [17]. RNA-seq data from the remaining 29 patients served as a validation cohort. Clinical information including the patient's age, gender, gross resection rate, primary or recurrent tumor, and the patient's follow-up information, was also collected. Six skull base chordoma samples were collected for single-cell RNA sequencing (scRNA-seq). Fresh skull base chordoma specimens were dissected into small pieces and digested into single-cell suspensions. The cell suspension was loaded into Chromium microfluidic chips with 3' v2 chemistry and barcoded with a 10× Chromium Controller (10X Genomics). The cDNA library was constructed with reagents from a Chromium Single Cell 3' v2 reagent kit (10X Genomics) and subsequently sequenced with Illumina NovaSeq 6000 by Novogene Bio Technology Inc (Tianjin, China). Reads for raw sequencing data were processed with Cell Ranger software (version 4.0.0). 224 BM-related genes were retrieved as sugguested by previous research suggested [6], and the specific BM-related genes are shown in Supplementary Table.

Construction and validation of a prognostic signature based on BM-related genes

We first analyzed the prognostic value of BM-related genes by univariate Cox regression analysis and obtained 16 survival genes ($p < 0.05$). The STRING database (http://www.string-db.org/) was used to analyze the pro tein-protein interactions (PPI) of 16 survival BM-related genes. Then using the "glmnet" R package, five genes were eventually obtained by least absolute shrinkage and selection operator (LASSO) regression analysis to construct a prognostic risk signature [18]. The risk score was calculated by the following equation:

Risk score = $\sum$ (expression of gene * coef).

Where coef was the LASSO Cox regression signature coefficient for the corresponding gene. Based on the median risk score, skull base chordoma patients of training and validation cohorts were divided into high-risk and low-risk groups respectively. We used the "FactoMineR" and "factoextra" R packages to perform principal component analysis (PCA) and used the "survival" and "survminer" R packages to evaluate the survival rates of patients in the two groups with Kaplan - Meier (KM) curves. The diverse characteristics of the

above five genes were visually represented in a circus plot using the "circlize" R package.

Differentially expressed genes (DEGs) analysis and functional enrichment analysis

Raw transcriptome counts data of skull base chordoma patients in the training cohort were prepared. The "limma" R package was used to perform DEGs analysis between high-risk and low-risk groups ($p < 0.05$,|log fold change(FC)|>1) [19]. Then, we used the "clusterProfiler" R package to perform Gene Ontology (GO) and Kyoto Encyclopedia of Genes and Genomes (KEGG) pathway analyses of DEGs [20–22]. In addition, GSEA software was used to analyze the KEGG pathways between different groups (|NES|>1, NOM p.value < 0.05, FDR < 0.25) [23].

Unsupervised clustering of Chordomas using BM-related genes

According to the crucial 5 BM-related genes, we used the "ConsensusClusterPlus" package to complete consensus clustering (CC) to identify the unidentified subtypes of skull base chordoma [24].

Construction of a nomogram

Clinical information and risk score were analyzed by univariate and multivariable Cox regression analysis. Then a nomogram including the risk score was developed to estimate the probability of 2-, 3-, and 4-year RFS. The nomogram plot was shown by the "regplot" R package. Calibration plots and decision curve analysis (DCA) were used to evaluate the efficacy with the "caret" and "rmda" R package. The "timeROC" R package was employed to generate receiver operating characteristic (ROC) curves.

Estimation of tumor immune microenvironment and drug sensitivity

The TIMER2.0 database (http://timer.cistrome.org/) was used to estimate immune cell infiltration. Estimation of Stromal and Immune Cells in Malignant Tumor Tissues using Expression Data (ESTIMATE) algorithm was used to assess tumor purity, immune infiltration, and stromal infiltration in skull base chordomas [25]. Moreover, to predict the effect of immune checkpoint therapy, the expression levels of several immune checkpoints were compared between different groups. Based on the Genomics of Drug Sensitivity in Cancer (GDSC, https://www.cancerrxgene.org/), we obtained half-maximal inhibitory concentration (IC50) estimates for specific drug using the "oncoPredict" R package to analyze drug sensitivity in different risk groups [26].

scRNA-seq analysis

The analysis of single-cell RNA sequencing data was undertaken with the "Seurat" and "SingleR" packages, following a series of standard quality procedures that included the "PercentageFeatureSet", "SCTransform", "RunPCA", "FindNeighbors", "FindClusters", "RunUMAP", and "FindMarkers" functions [27]. Cell types were assigned using known markers from the literature [16].

Cell lines, cell culture, and transfection

The human chordoma cell line UM-Chor1 was purchased from the American Type Culture Collection (ATCC), and MUG-Chor1 cells were kindly provided by the Chordoma Foundation. Cells were cultured in a mixture of IMDM (ATCC) and RPMI-1640 (ATCC) culture media (4:1) supplemented with 10% fetal bovine serum, while the culture medium of MUG-Chor1 cell line was additionally supplemented with 1% L-glutamine. All cells were cultured in an incubator 5% CO2 incubator at 37 °C. Small interfering RNA (siRNA) targeting ITGB3 (siITGB3) and negative control (siNC) was obtained from RiboBio (Guangzhou, China). Cells were transfected using Lipofectamine 3000 (Invitrogen) 24 h after seeding.

Cell counting Kit-8 (CCK-8) and colony formation assays

Cell viability was evaluated using CCK-8 (Dojindo, Japan). Briefly, 2×10^3 UM-Chor1 cells per well and 6×10^3 MUG-Chor1 cells per well were seeded in a 96-well plate. CCK-8 was added at 1, 2, and 3 days, and absorbance at 450 nm was then measured. For colony formation assays, 2×10^3 transfected chordoma cells were seeded in a six-well plate and incubated for 14 days. Colonies were then fixed with 4% paraformaldehyde, and stained with crystal violet.

Transwell migration assay

Briefly, 4×10^4 UM-Chor1 cells or 1×10^5 MUG-Chor1 cells were incubated in an 8.0-μm Transwell chamber (Corning) after transfected. After 24 h, the migrated chordoma cells at the lower surface were fixed with 4% paraformaldehyde and stained with crystal violet.

Western blot

Transfected UM-Chor1 cells and MUG-Chor1 cells were lysed in RIPA lysis buffer containing protease and phosphatase inhibitors. For Western blot, protein samples (20 μg) were separated by SDS-PAGE and then transferred to polyvinylidene difluoride membranes. After being blocked with 5% TBST skimmed milk for 2 h, the polyvinylidene difluoride membranes were incubated with the primary antibodies targeting ITGB3 (13166, Cell Signaling Technology, 1:1000), Akt (75692, Cell Signaling Technology, 1:1000), phospho-Akt (Ser473, 9018, Cell Signaling Technology, 1:1000), and GAPDH (TA-08,

ZSGB-BIO, 1:8000). After incubation with primary antibody overnight, the membrane was washed with TBST and incubated with secondary antibody tagged with horseradish peroxidase (Santa Cruz Biotechnology). Protein bands were visualized by enhanced chemiluminescence assay using an imaging apparatus (Amersham Imager 600, GE).

RNA extraction and qRT-PCR

Total RNA was isolated from chordoma cells using RNeasy Mini Kit (Qiagen, GE), and the Evo M-MLV RT Premix for qPCR (Accurate Biology, CHINA) was used to synthesize cDNA. qRT-PCR was conducted on a QuantStudio 5 (Applied Biosystems) in triplicate and GAPDH was selected as the experimental reference. All primers were synthesized by Sangon Biotech (Shanghai, China). Primer sequences were as follows: ITGB3 forward, 5'-AGTAACCTGCGGATTGGCTTC-3' and reverse, 5'-GTCACCTGGTCAGTTAGCGT-3'; GAPDH forward, 5'-ACAACTTTGGTATCGTGGAAGG-3' and reverse, 5'-GCCATCACGCCACAGTTTC-3'.

Statistical analysis

All statistical analyses were performed with R software (version 4.3.2). Kaplan-Meier (KM) analysis and Cox analysis were implemented with the "survival" and "survminer" R package. Wilcox test was used to compare the difference in risk scores between different clinical characteristics. Spearman's rank correlation coefficient was used for correlation analysis. The correlation figures are plotted with the "ggplot2" R packages. $P<0.05$ was considered significant. This research is reported in line with the REMARK criteria [28].

Results

Construction of the prognostic signature for BM-related genes

The methodology of the study is illustrated in Fig. 1. In the training cohort, we performed univariate Cox regression analysis for 224 BM-related genes and found 16 survival genes related to RFS (Fig. 2A). Among them, only SMOC1 was protective factors (hazard ratio, HR < 1), while COL12A1, COL13A1, COL4A1, COL4A2, ITGB3, ROBO4, SERPINF1, ADAMTS5, ADAMTS8, COL14A1, LOXL2, POSTN, SLIT2, THBS2 and UNC5B (HR > 1) were risk factors. The STRING database was used to construct a PPI network that showed the complex relationship between these prognostic indicators in skull base chordoma (Fig. 2B) and the correlation between the expression of each gene was investigated (Supplementary Fig. 1).

Using LASSO regression analysis, we identified five genes with non-zero penalty coefficients and established a signature that predicted the prognosis of skull base chordoma patients (Fig. 2C-D), which included UNC5B, COL14A1, COL13A1, SMOC1, and ITGB3. The chromosomal location of each gene is depicted (Fig. 2E). Kaplan-Meier analysis was used to determine their respective influence on the RFS time (Supplementary Fig. 2A). The risk coefficients were calculated from the correlation coefficients of the 5 BM-related genes with the following formula:

Risk score = (0.04107 * UNC5B expression) + (0.02979 * COL14A1 expression) + (0.06416 * COL13A1 expression) + (-0.11697 * SMOC1 expression) + (0.02623 * ITGB3 expression).

The training cohort was divided into the high-risk group ($n=24$) and the low-risk group ($n=24$) based on the median risk score. The heatmap showed different expression levels of 5 BM-related genes and clinic features in the two subgroups of 48 chordoma patients (Fig. 2F). We also analyzed the association between risk score and clinical features including age, gender, and primary or recurrent tumor. Patients older than 50 had a higher risk score than those younger than 50 while gender and primary or recurrent tumor were not associated with the risk score (Supplementary Fig. 3B).

Differential gene analysis and function analysis between high-risk and low-risk groups

The "Limma" R package was used to analyze the DEGs between two groups, resulting in the identification of 2157 DEGs ($p<0.05$,|log FC| > 1), of which 1721 up-regulated genes and 436 down-regulated genes in high-risk group (Fig. 2G). GO analysis and KEGG analysis of up-regulated genes in the high-risk group were then performed (Fig. 2H-I). GO analysis indicated that genes were mainly enriched in terms associated with the extracellular matrix. The KEGG analysis results indicated several pathways involving tumor malignancy progression, such as the PI3K-Akt signaling pathway, Rap1 signaling pathway and Wnt signaling pathway.

GSEA analysis was used to further unravel the molecular mechanisms underlying the signature of BM-related genes (Supplementary Fig. 3A-B). The results showed that antigen processing and presentation, IL-17 signaling pathway, NF-kappa B signaling pathway, p53 signaling pathway and viral protein interaction with cytokine and cytokine receptor were mainly enriched in the high-risk group. The results of GSEA analysis suggested that BM-related gene signature are likely to be associated with oncogenic pathways, cell-cell interactions and the tumor immune microenvironment.

Unsupervised clustering of BM-related signature genes

To explore unidentified subtypes of skull base chordoma, 5 BM-related model genes were used to perform the CC analysis. We found that when k = 2, the differences among

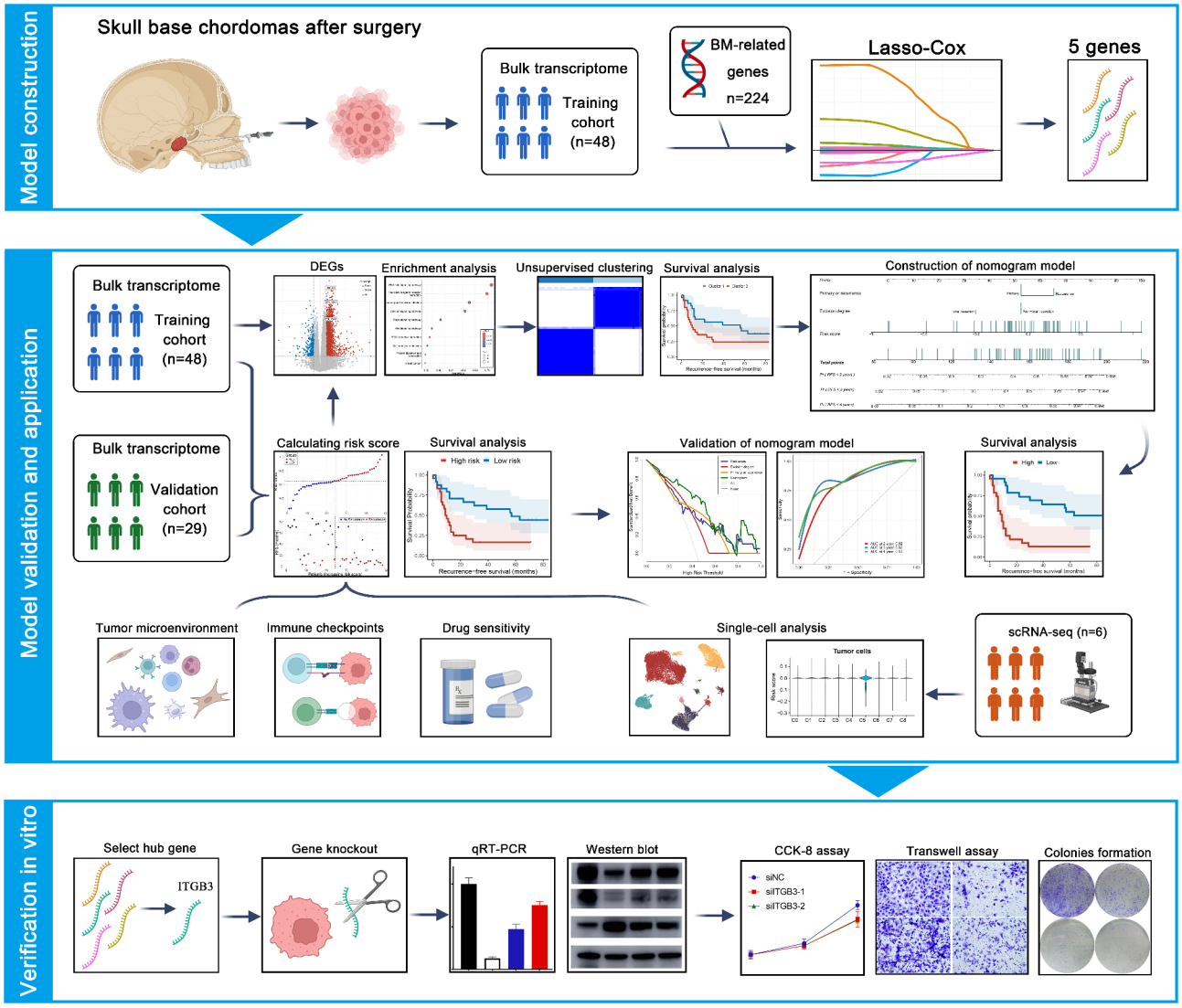

Fig. 1 Methodology of the study

subgroups were most obvious, which indicated that the 48 skull base chordoma patients in the training cohort could be well classified into two clusters (Fig. 3A-B). The alluvial diagrams showed that the majority of cluster 2 was associated with high risk score, whereas the majority of cluster 1 was related to low risk score (Fig. 3C). An obvious difference was found between RFS times of the two clusters ($p = 0.044$, Fig. 3D). Specifically, cluster 1 was related to favorable prognosis, whereas cluster 2 was associated with adverse prognosis.

Internal training and external validation of the gene signature prediction model

Utilizing the calculated risk score, we stratified 48 skull base chordoma patients in the training cohort into high-risk and low-risk groups. Our results revealed that patients with high risk scores had a lower RFS rate than those with low risk scores (Fig. 3E). PCA showed that the classification was satisfactory based on risk score (Fig. 3F). A marked difference was detected in the RFS time between these two groups. The low-risk group was related to a favorable prognosis, whereas the high-risk group was associated with a poor prognosis ($p = 0.0038$, Fig. 4G). Subsequently, we used another 29 skull base chordoma patients as the validation cohort. Simliarly, patients in the validation cohort were divided into two groups (Fig. 3E). Furthermore, the two groups were satisfactorily separated using PCA (Fig. 3F). KM analysis also showed that the patients in the high-risk group were more likely to have a shorter RFS and higher recurrence rates ($p = 0.021$, Fig. 3G).

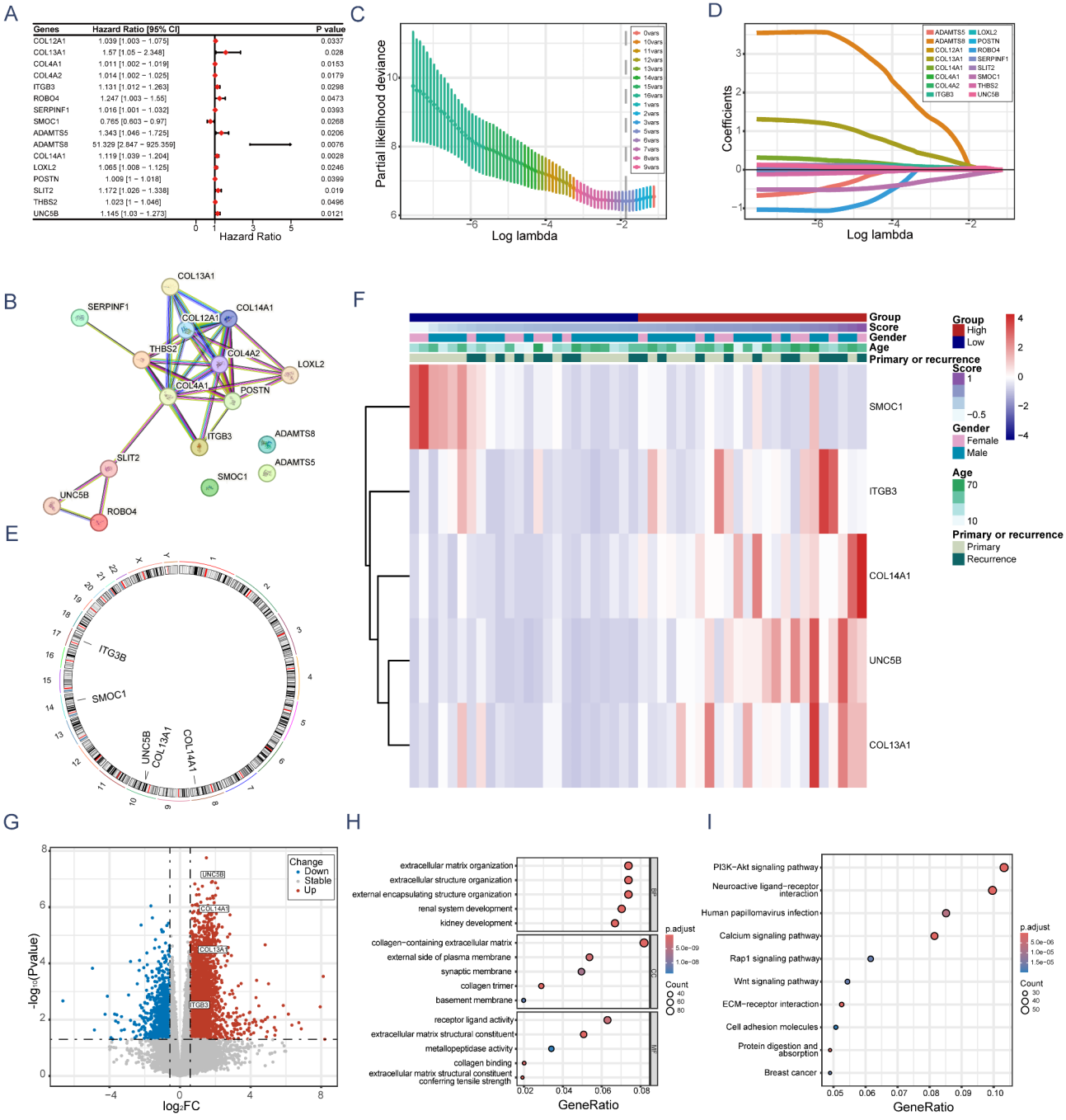

Fig. 2 Establishment of the BM-related genes signature in skull base chordoma. (**A**) Univariate Cox regression analysis showing the prognostic values of BM-related genes. (**B**) A PPI network of prognostic BM-related genes. (**C**) Gene coefficient spectrum of the 21 prognostic BM-related genes in the LASSO regression analysis. (**D**) Selection of the optimal penalty parameter in the LASSO Cox regression model. (**E**) Circos plot depicting the locations of five model genes. (**F**) A heatmap showed the relationship between risk score, the model genes, and clinicopathological features. (**G**) Volcano map showed differentially expressed genes (DEGs) between high-risk and low-risk groups. (**H**) GO analysis of up-regulated genes in high-risk group. (**I**) KEGG analysis of up-regulated genes in high-risk group

Development and assessment of the nomogram survival model

The univariate Cox regression analysis showed that risk score was regarded as a risk factor (HR = 13.685, 95% CI: 3.929–47.663, and $p < 0.001$, Fig. 4A). Besides risk score, recurrence tumor was regarded as a risk factor (HR = 2.848, 95% CI: 1.42–5.713, and $p = 0.003$) while total resection was regarded as a protective factor (HR = 0.277, 95% CI: 0.096–0.797, and $p = 0.017$, Fig. 4A). In the multivariate Cox analysis, risk score retained its

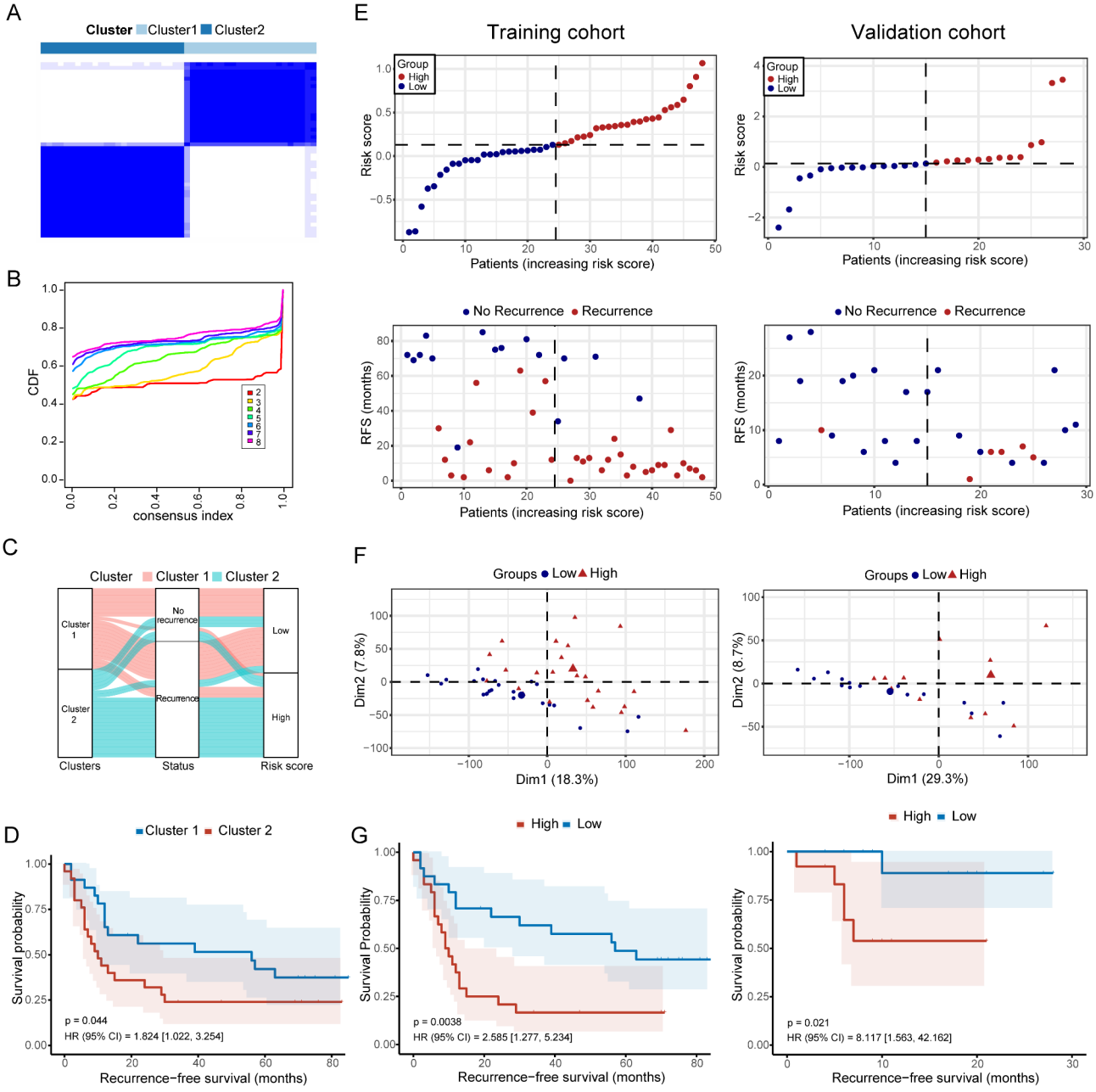

Fig. 3 Internal training and external validation of the gene signature prediction model. (**A**) Training cohort patients were grouped into two molecular clusters when k = 2 based on the BM-related model gene profile. (**B**) Empirical cumulative distribution function plot displaying consensus distributions for each k value (from 2 to 8). (**C**) Alluvial diagram shows the interrelationship between molecular clusters, survival status, and risk groups. (**D**) Kaplan-Meier curves show the recurrence-free survival between two different molecular clusters. (**E**) Distribution of risk score according to the survival status and time in training and validation cohorts. (**F**) Principal component analysis plot based on the training and validation cohorts. (**G**) Kaplan-Meier curves show recurrence-free survival between two risk groups of training and validation cohorts

independent prognostic value in skull base chordoma patients after adjusting for other confounding factors (HR = 12.995, 95% CI: 3.312–50.99, $p < 0.001$, Fig. 4B).

Multivariable Cox and stepwise regression analyses were used to establish a nomogram model in the training cohort to estimate the 2-, 3-, and 4-year RFS. The risk score, degree of resection, and primary or recurrence were included in the model (Fig. 4C). The calibration curves demonstrated the accurate predictive ability of this nomogram model for the 2-, 3-, and 4-year RFS rates (Fig. 4D). Significant RFS difference was found between the high-point and low-point groups based on the nomogram ($p < 0.0001$, Fig. 4E). Additionally, we evaluated the area under curve (AUC) values of ROC curves in the

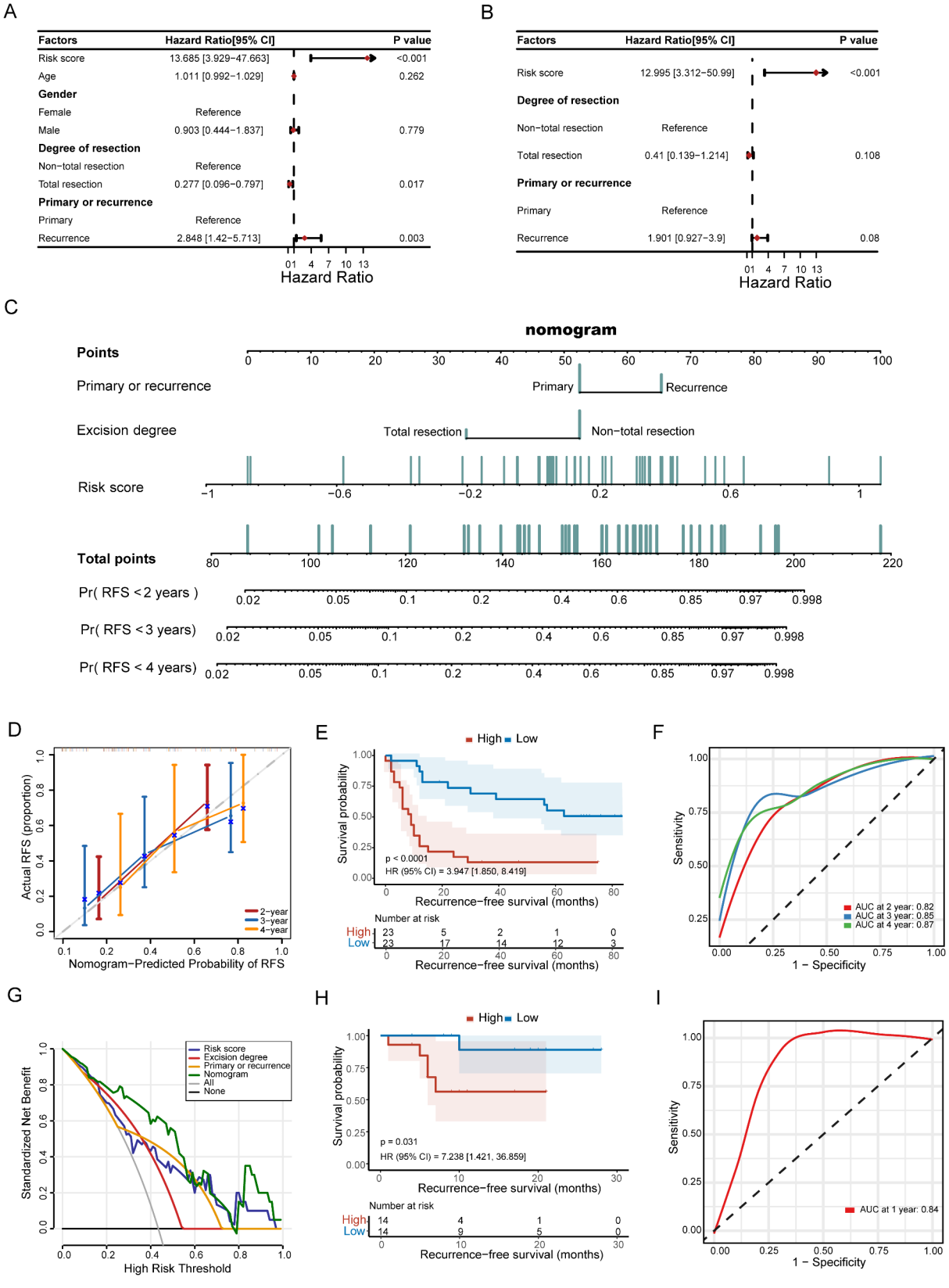

Fig. 4 (See legend on next page.)

(See figure on previous page.)

Fig. 4 Establishment and assessment of the nomogram survival model. (**A**) Univariate analysis for the clinicopathologic characteristics and risk score. (**B**) Multivariate analysis for the clinicopathologic characteristics and risk score. (**C**) A nomogram was established to predict the prognostic of skull base chordoma patients. (**D**) Calibration plots showing the probability of 2-, 3-, and 4-year recurrence-free survival in the training cohort. (**E**) Kaplan-Meier analyses for the two groups based on the nomogram point in the training cohort. (**F**) Receiver operator characteristic (ROC) analysis of nomogram in the training cohort. (**G**) Decision curve analysis (DCA) of the nomogram predicting recurrence-free survival. (**H**) Kaplan-Meier analyses for the two groups based on the nomogram score in the validation cohort. (**I**) ROC analysis of nomogram in the training cohort

training cohort, and the results showed that the nomogram had high accuracy in predicting 2-, 3-, and 4-year survival of skull base chordoma patients (Fig. 4F). Moreover, DCA confirmed that the nomogram model outperformed other predictors utilized in the study (Fig. 4G).

To evaluate the performance of the nomogram model, we accessed its predictive ability in the validation cohort. KM analysis demonstrated that the patients in the high-point group were more likely to have a shorter RFS and higher recurrence rates (Fig. 4H). Although the follow-up time in the validation cohort was short, the AUC showed that the nomogram had high accuracy in predicting 1-year recurrence-free survival of skull base chordoma patients (Fig. 4I).

The association between BM-related signature and tumor immune

A variety of algorithms including TIMER, CIBERSORT, CIBERSORT-ABS, QUANTISIEQ, XCELL, EPIC, MCP-COUNTER, and ESTIMATE were used to comprehensively measure the enrichment scores of cells in the microenvironment of the skull base chordoma (Supplementary Fig. 4). We analyzed the correlation of the risk score with various enrichment scores of immune cells. Cells that significantly correlate with risk scores ($p < 0.05$) are shown Fig. 5A. Strikingly, enrichment scores for CAF of 3 different algorithms (XCELL, EPIC, and MCP-COUNTER) were positively correlated with the risk score, indicating a close relationship between CAF and BM-related genes. In addition, immunosuppressive cells such as M2-like macrophages and Treg cells showed a significant positive correlation with the risk score, suggesting the presence of immunosuppressive microenvironment in the skull base chordoma with a high risk score. Using the ESTIMATE algorithm, we found that the ESTIMATE score, immune score, and stromal score were higher in the high-risk group and positively correlated with the risk score (Fig. 5B-D).

We investigated the relationship between immune checkpoint molecules, risk score, and the model gene expression levels. The results showed that the expression of TNFSF4, TNFSF18, TNFRSF4, PDCD1LG2, HAVCR2, and CTLA4 were all significantly positively correlated with risk score ($p < 0.05$), indicating the presence of immunosuppressive microenvironment in the high-risk group (Fig. 5E). In summary, these findings provide valuable insights into the intricate interplay between BM-related signature, immune cell infiltration, and immune checkpoint regulation in skull base chordoma.

Analysis of BM-associated signature with scRNA-seq

To probe the distribution of BM-related signature at a single-cell resolution, we scrutinized the scRNA sequencing data of 6 skull base chordoma patients. After employing various standard quality control procedures, a total of 81,973 cells were included for downstream analysis. The major cell types were annotated (Fig. 6A-B) and the expression of representative genes for the six cellular subpopulations was shown (Fig. 6D). Next, we investigated contributions of various cell types to bulk BM signature. We calculated the BM-associated risk score for each cell and found that fibroblasts and partial tumor cells were major contributors to the overall risk score (Fig. 6C). To investigate the heterogeneity among tumor cells, we further conducted a dimensionality reduction analysis of all tumor cells. We identified nine tumor cell subclusters and only C3 had a significantly lower risk score than the other subclusters (Fig. 6E-F). Further analysis revealed that down-regulated genes of C3 were enriched in the classical oncogenic pathway including the PI3K-Akt signaling pathway, TGF-beta signaling pathway, MAPK signaling pathway, and p53 signaling pathway (Fig. 6G).

The association between BM-related signature and drug sensitivity

To explore the potential relationship between the risk score and drug sensitivity, we analyzed IC50 values for several drugs using the GDSC database. The correlation and significance between the IC50 of various drugs and the risk score are presented (Fig. 7A). Interestingly, we found that the IC50 values of palbociclib, lapatinib, nilotinib, oxaliplatin, sorafenib, and vinblastine were lower in the high-risk group (Fig. 7B). These findings suggest a potential association between our model genes and drug sensitivity, providing valuable insights for personalized treatment strategies in skull base chordoma.

ITGB3 promotes the proliferation, migration, and colony formation of chordoma cells

Among the five BM-related genes mentioned above, ITGB3 was selected for further analysis given that ITGB3 was the only gene associated with overall survival (OS) of chordoma patients ($p < 0.05$, Supplementary Fig. 5A). Differential gene analysis and functional enrichment analysis

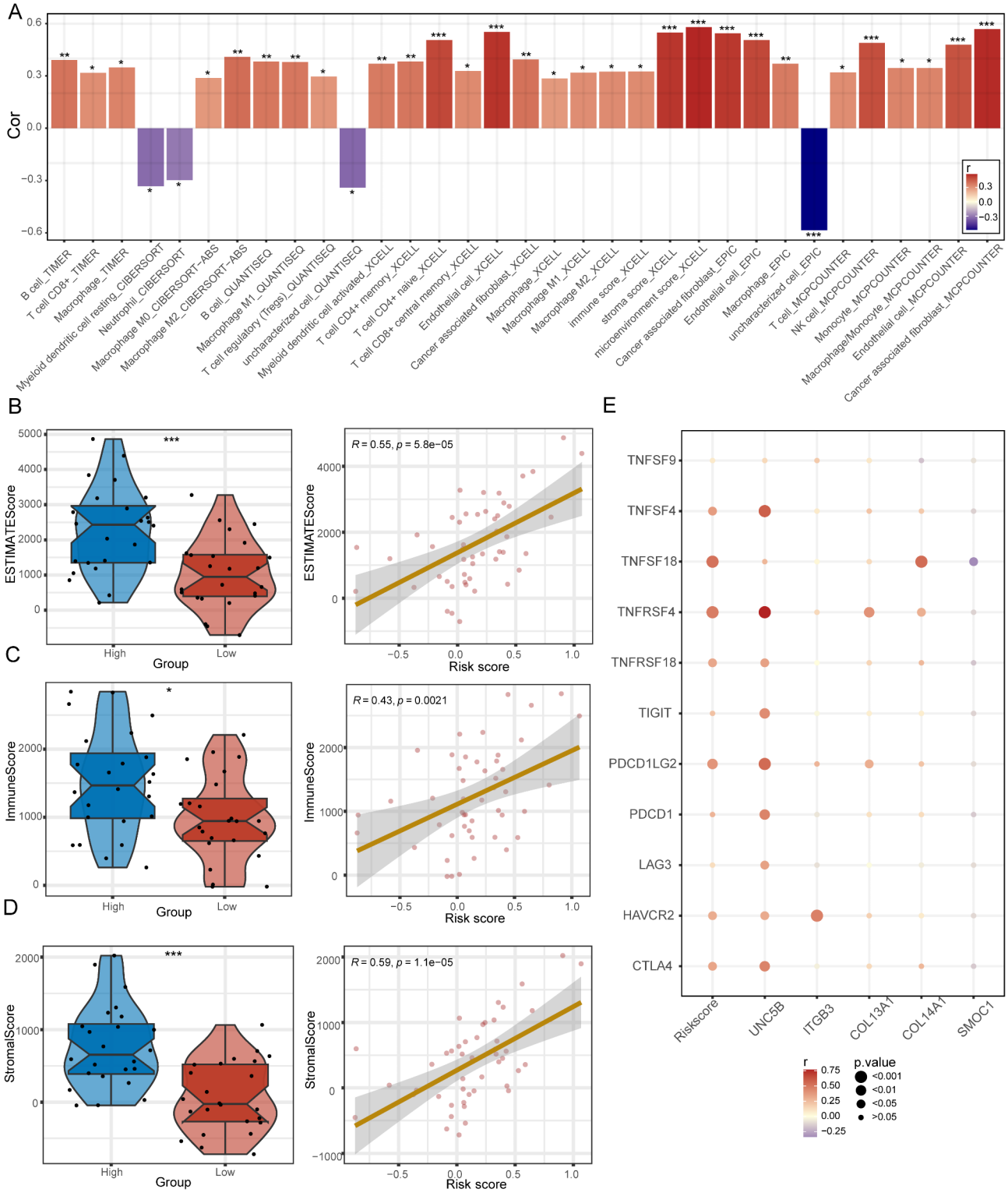

Fig. 5 Dissection of tumor microenvironment based on BM-related signature. (**A**) Bar plot of the relationship between immune cells and risk score based on the different algorithms. (**B**) Boxplots and correlation plots of the relationship between the ESTIMATEScore and risk score. (**C**) Boxplots and correlation plots of the relationship between the ImmuneScore and risk score. (**D**) Boxplots and correlation plots of the relationship between the StromalScore and risk score. (**E**) Bubble plot of the relationship between immune checkpoints, risk score, and model genes. *, *p*-value < 0.05; **,*p*-value < 0.01; ***, *p*-value < 0.001

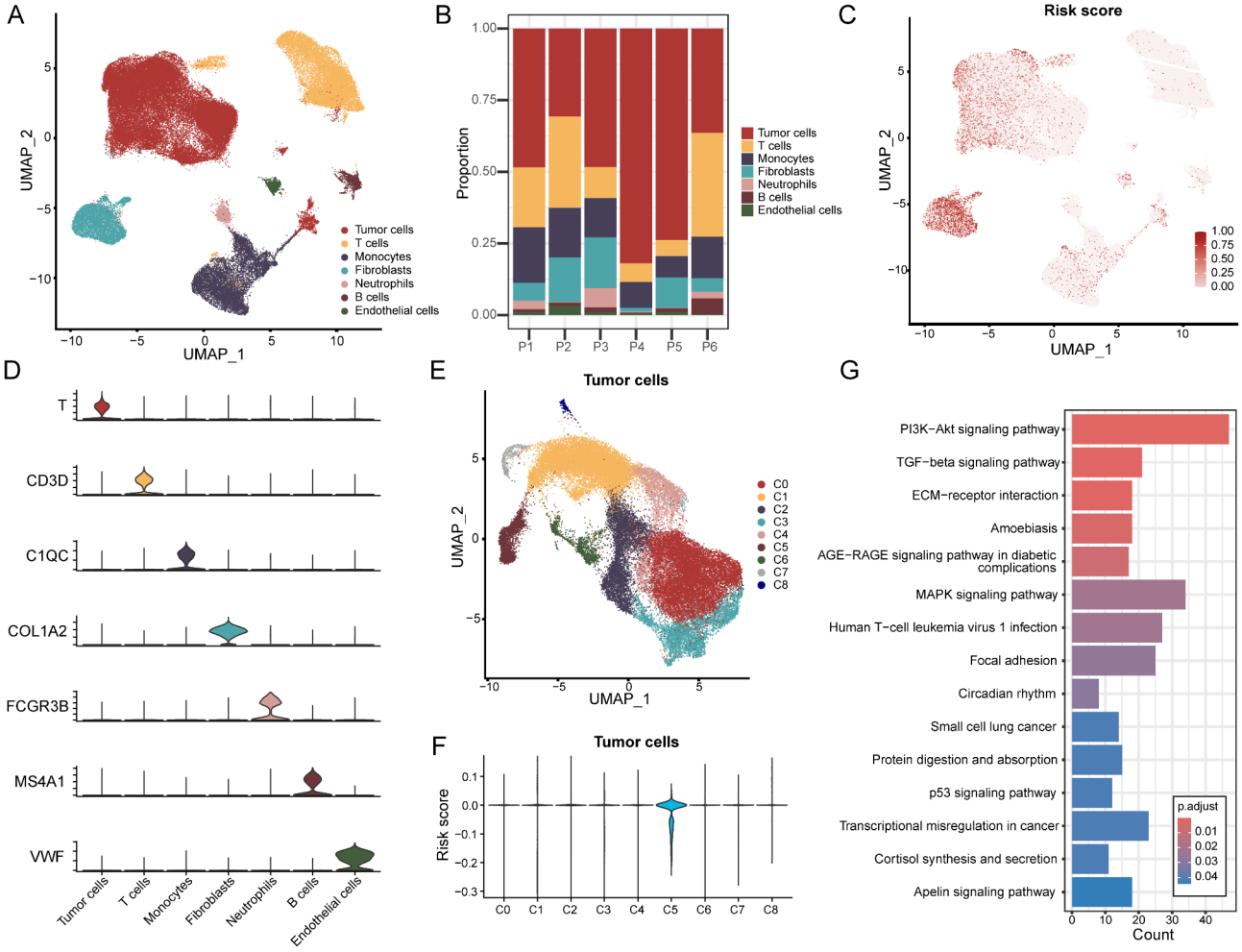

Fig. 6 Analysis of BM-associated signature with scRNA-seq. (**A**) UMAP plot visualization of all cell types from six skull base chordoma samples. (**B**) Proportion of cell subtypes in six samples. (**C**) UMAP plot visualization of the distribution of normalized risk score. (**D**) Violin plot of representative markers in different cell types. (**E**) UMAP plot visualization of tumor cell subtypes. (**F**) Violin plot of risk score in different tumor cell subclusters. (**G**) KEGG analysis of down-regulated genes in C3 cluster

suggested the classical oncogenic PI3K-Akt signaling pathways were found to be enriched in the ITGB3 high-expression group (Fig. 8A-B, Supplementary Fig. 5B-C).

Three siRNAs (siITGB3-1, siITGB3-2, and siITGB3-3) were then used to knockdown ITGB3 in two chordoma cell lines UM-Chor1 and MUG-Chor1. The qRT-PCR and Western blot showed that ITGB3 expression was significantly reduced in UM-Chor1 and MUG-Chor1 cells after transfection with siITGB3-1 or siITGB3-2, while siITGB3-3 has a poor silencing efficiency (Fig. 8C-E). Consequently, siITGB3-1 and siITGB3-2 were chosen for the subsequent experiments to explore the effect of ITGB3 on chordoma cells. CCK-8 and colony formation assays suggested that knockdown ITGB3 inhibited the proliferation and colony forming abilities of UM-Chor1 and MUG-Chor1 cells (Fig. 8F-I). In addition, the silencing of ITGB3 significantly inhibited the migration of chordoma cells (Fig. 8J-K). Western blot showed that the phospho-Akt level of chordoma cells was reduced after the knockdown of ITGB3, suggesting that ITGB3 may promote chordoma progression through the PI3K-Akt pathway, which is consistent with the results of the functional enrichment analysis above (Fig. 8E). Collectively, our results demonstrate that ITGB3 could promote chordoma cell growth and migration via the PI3K-Akt pathway.

Discussion

In this study, we utilized LASSO Cox regression analysis to identify five BM-related genes and construct a prognostic model for skull base chordoma. The accuracy of the model was validated in an independent cohort. Based on the median risk score, patients were classified into the high-risk group with a poor prognosis and the low-risk group with a favorable prognosis. Differential gene analysis between these groups, followed by functional

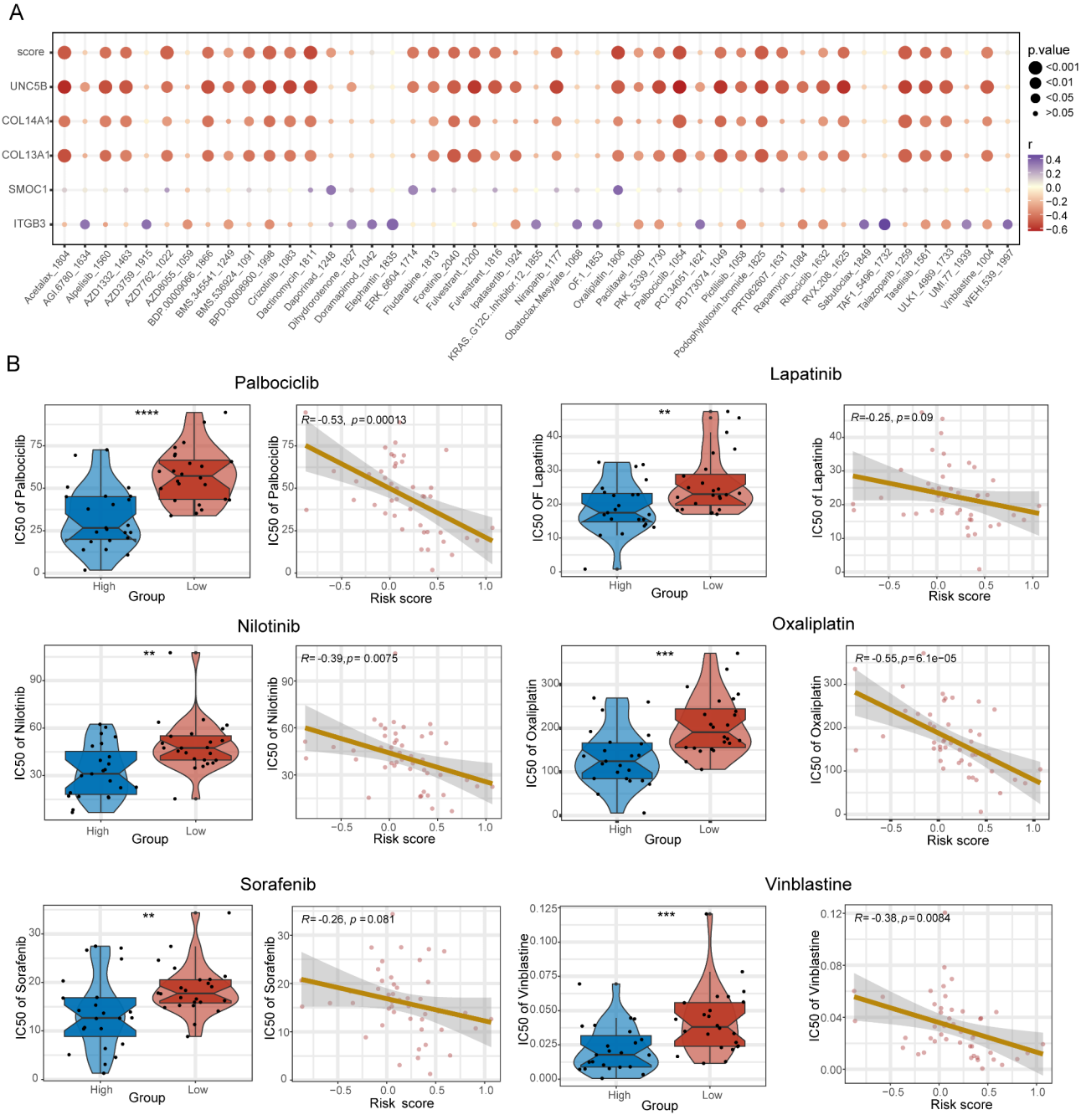

Fig. 7 Drug sensitivity analysis based on BM-related signature. (**A**) Bubble plot of the relationship between IC50, risk score, and model genes. (**B**) Boxplots of the comparison of IC50 of drugs between high- and low-risk groups, and correlation between the IC50 and risk score. *, *p*-value < 0.05; **, *p*-value < 0.01; ***, *p*-value < 0.001

enrichment analysis were conducted to investigate the role of BM-related genes in chordoma. A nomogram incorporating clinical features and risk score was developed, and its clinical utility of this model was validated. Additionally, the risk score was strongly correlated with immune cell infiltration and drug sensitivity. We further selected ITGB3 for in vitro validation and found that its knockdown significantly inhibited the proliferation, migration, and colony formation of chordoma cells.

BM-related genes are widely present in the organism, and their expression products are involved in the composition of the extracellular matrix, which is closely related to the occurrence of malignant tumors and recurrent metastasis [9]. Currently, no study focused on BM-related genes in chordoma, this study is a preliminary

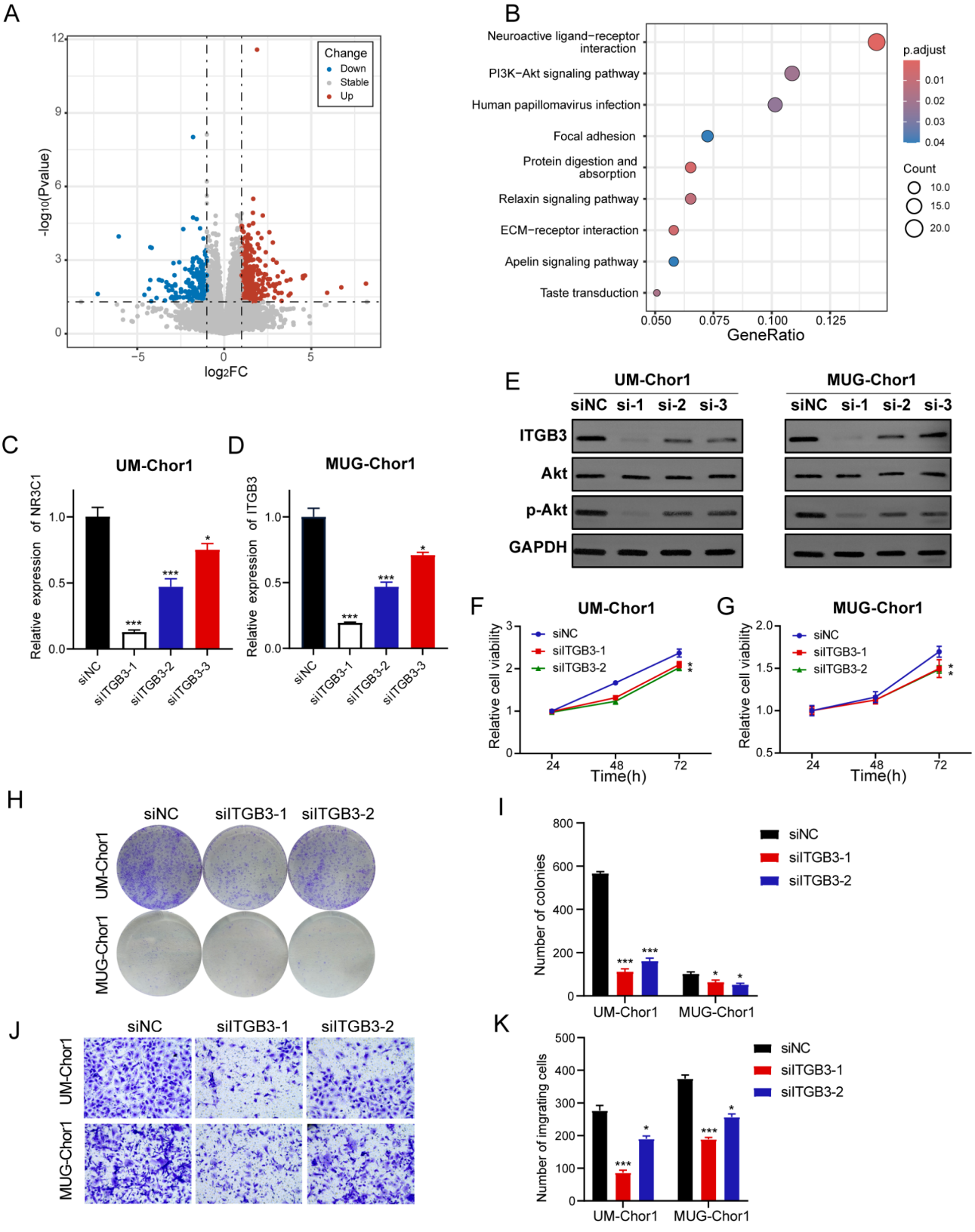

Fig. 8 (See legend on next page.)

(See figure on previous page.)

Fig. 8 ITGB3 knockdown inhibited the proliferation and migration of chordoma cells in vitro. (**A**) Volcano map showed DEGs between ITGB3 high and low expression groups. (**B**) KEGG analysis of up-regulated genes in ITGB3 high expression group. (**C-D**) qRT-PCR validation in chordoma cells with or without ITGB3 knockdown. (**E**) The protein expression of ITGB3 and AKT in chordoma cells with or without ITGB3 knockdown. (**F-G**) CCK8 results of chordoma cells with or without ITGB3. (**H-I**) The migration cells were significantly reduced in chordoma cells with ITGB3 knockdown. (J-K) The number of cell colonies significantly decreased in chordoma cells with ITGB3 knockdown. *, p-value < 0.05; **, p-value < 0.01

exploration of BM-related genes in chordoma. We created a signature featuring five BM-related genes (ITGB3, SMOC1, UNC5B, COL14A1, and COL13A1) and found that it could predict RFS of skull base chordoma patients. Among five prognostic genes, all have been reported to be related to the malignant progression of cancers. Integral proteins, ubiquitously found on the surface of vertebrate cells, mediate mutual recognition and adhesion between cells and cells and between cells and the extracellular matrix [29]. ITGB3, a member of the integrin family, has been reported in various tumors including hepatocellular carcinoma, nasopharynx cancer, and colon cancer, and plays a critical role in tumor cell proliferation, migration, invasion, metastasis, and angiogenesis [30–33]. In this study, we focused on the relationship between ITGB3 and the PI3K-Akt signaling pathway. However, ITGB3 may also exert oncogenic effects through other mechanisms, such as ferroptsis and intercellular communication [31, 33]. Future studies should investigate these additional signaling networks to further elucidate their potential contributions to tumor biology and prognosis in chordoma. SMOC1 encodes a secreted modular glycoprotein and is involved in embryogenesis, endothelial cell proliferation, angiogenesis, integrin–matrix interactions, and cell adhesion [34–36]. In the current study, SMOC1 was the only one of the five crucial genes whose high expression was positively associated with favorable prognosis, which is consistent with one previous research in gliomas [37]. UNC5B, as a member of UNC5 axon guidance gene family, was involved in neuronal growth as an NTN-binding receptor and performed a dual role in apoptosis [38–40]. Due to its effects on apoptosis and cell survival, UNC5B is implicated to be closely related to tumorigenesis. UNC5B is aberrantly expressed in a variety of cancers, including colorectal, bladder, and breast cancer [41–43]. Collagen is widely distributed in organisms, and collagen type IV is the most important structural component of the basement membrane [44]. COL14A1 has been reported to have a high mutation prevalence and an unexpectedly high incidence of nonsynonymous mutations in gastric cancer, leading to a poor prognosis [45]. In addition, COL14A1 was one of the effective biomarkers for predicting peritoneal metastasis of gastric cancer [46]. Moreover, it was reported that overexpressed COL13A1 contributes to the proliferation and migration of bladder cancer cells [47].

To further investigate the biological mechanisms potentially relevant to the prognostic risk assessment of BM-related genes, we performed functional enrichment analysis of DEGs between these groups. It was found that cell adhesion molecules, ECM-receptor interaction, and some classical carcinogenic pathways such as the PI3K-Akt signaling pathway, the Rap1 signaling pathway, and the Wnt signaling pathway were significantly enriched in the high-risk group, which were associated with tumor proliferation, metastasis, and treatment resistance [48–51].

Tumor cells can promote their survival and development by mediating immune escape and resisting drug treatments. The tumor microenvironment is the important constituent of the tumor stroma and critically takes part in tumor survival and progression [52]. Understanding the cross-talk between cancer cells and tumor microenvironment will allow for improving therapeutics and increasing the likelihood of favorable patient outcomes. We evaluated the tumor immune cell infiltration enrichment score by multiple algorithms. The results showed that CAFs were significantly and positively associated with the risk score. CAFs have been shown to play several roles in tumer development. They secrete growth factors, inflammatory ligands, and extracellular matrix proteins that promote cancer cell proliferation, therapy resistance, and immune exclusion [53]. Furthermore, the expression of several immune checkpoints was higher in the high-risk group than in the low-risk group suggesting chordoma patients in the high-risk group may benefit more from immune checkpoint inhibitor therapy. Moreover, we explored the sensitivity of different risk groups to specific chemotherapeutic agents, and the results revealed a lower IC50 values of these chemotherapeutic agents in the higher-risk groups. In conjunction with the above analysis of immune checkpoints, our data suggested chemotherapy combined with immunotherapy may be potentially valuable for chordoma patients with high BM risk score.

However, our study has several limitations. First, due to the rarity of chordoma, the sample size was relatively small which may impact the generalizability. To mitigate this limitation, we supplemented our findings with in vitro cellular experiments. We also discussed potential strategies for future studies, including the expansion of the sample size to validate our results. Specifically, a larger cohort and more extensive multi-omics data could be involved in future. In addition, due to the limitations of the sample size in this study, the clinical application

of this prognostic model requires a great deal of further work before it can be fully realized.

Conclusions

The BM-related genes signature conducted in this study is a practical prognostic predictor for postoperative skull base chordoma patients. And the hub BM-related gene ITGB3 may influence the malignant progression of chordoma via the PI3K-AKT signaling pathway.

Abbreviations

BM	Basement membrane
CAF	Cancer-associated fibroblasts
RFS	Recurrence-free survival
RNA-seq	RNA-sequencing
scRNA-seq	Single-cell RNA sequencing
PPI	Protein-protein interactions
LASSO	Least absolute shrinkage and selection operator
PCA	Principal component analysis
DEGs	Differentially expressed genes
GO	Gene Ontology
KEGG	Kyoto Encyclopedia of Genes and Genomes
CC	Consensus clustering
DCA	Decision curve analysis
ROC	Receiver operating characteristic
ESTIMATE	Estimation of Stromal and Immune Cells in Malignant Tumor Tissues using Expression Data
GDSC	Genomics of Drug Sensitivity in Cancer
siRNA	Small interfering RNA
AUC	Area under curve
IC50	Half-maximal inhibitory concentration
OS	Overall survival

Supplementary Information

The online version contains supplementary material available at https://doi.org/10.1186/s12885-025-14006-1.

Supplementary Material 1

Supplementary Material 2

Supplementary Material 3

Supplementary Material 4

Supplementary Material 5

Supplementary Material 6

Supplementary Material 7

Acknowledgements

Not applicable.

Author contributions

T. Zhang and M. Li analyzed and interpreted the results and drafted the manuscript; Q. Liu, X. Liu and S. Zhao designed the process and procedure of the study; T. Zhang and M. Li performed the data curation and analysis; X. Zhang and Y. Liu compiled the clinical data; Y. Zhang and J. Bai reviewed and revised the analysis and manuscript.

Funding

This study was supported by the National Natural Science Foundation of China (82272939 and 82303938). This study sponsors had no such involvement.

Data availability

The RNA-Seq data generated in this study have been deposited in the Database of Genotypes and Phenotypes (dbGaP) under Accession Code phs002301.v1.p1. The remaining data is available upon request from the corresponding author.

Declarations

Ethics approval and consent to participate

The Ethics Committee of Beijing Tiantan Hospital, Capital Medical University, approved the study. Judgement's reference number: NO. 2009-47. All participants signed the informed consent form, and the study was conducted according to the Declaration of Helsinki principles.

Consent for publication

Not applicable.

Competing interests

The authors declare no competing interests.

Author details

[1]Beijing Neurosurgical Institute, Capital Medical University, No.119 South Fourth Ring West Road, Fengtai District, Beijing 100070, China
[2]Department of pathology, Beijing Tiantan Hospital, Capital Medical University, Beijing, China
[3]Department of Neurosurgery, Beijing Tiantan Hospital, Capital Medical University, Beijing, China
[4]Beijing Institute for Brain Disorders Brain Tumor Center, Beijing, China
[5]China National Clinical Research Center for Neurological Diseases, Beijing, China

Received: 17 December 2024 / Accepted: 24 March 2025
Published online: 03 April 2025

References

1. Ulici V, Hart J, Chordoma. A review and differential diagnosis. Archives Pathol Lab Med (1976). 2022;146(3):386–95.
2. McMaster ML, Goldstein AM, Bromley CM, Ishibe N, Parry DM. Chordoma: incidence and survival patterns in the united States, 1973–1995. Cancer Causes Control. 2001;12(1):1–11.
3. Wedekind MF, Widemann BC, Cote G, Chordoma. Current status, problems, and future directions. Curr Probl Cancer. 2021;45(4):100771.
4. Radaelli S, Stacchiotti S, Ruggieri P, Donati D, Casali PG, Palmerini E, et al. Sacral Chordoma: Long-term outcome of a large series of patients surgically treated at two reference centers. Spine (Phila Pa 1976). 2016;41(12):1049–57.
5. Chang J, Chaudhuri O. Beyond proteases: basement membrane mechanics and cancer invasion. J Cell Biol. 2019;218(8):2456–69.
6. Jayadev R, Morais M, Ellingford JM, Srinivasan S, Naylor RW, Lawless C, et al. A basement membrane discovery pipeline uncovers network complexity, regulators, and human disease associations. Sci Adv. 2022;8(20):eabn2265.
7. Pozzi A, Yurchenco PD, Iozzo RV. The nature and biology of basement membranes. Matrix Biol. 2017;57–58:1–11.
8. Sherwood DR. Basement membrane remodeling guides cell migration and cell morphogenesis during development. Curr Opin Cell Biol. 2021;72:19–27.
9. Gatseva A, Sin YY, Brezzo G, Van Agtmael T. Basement membrane collagens and disease mechanisms. Essays Biochem. 2019;63(3):297–312.
10. Banerjee S, Lo WC, Majumder P, Roy D, Ghorai M, Shaikh NK, et al. Multiple roles for basement membrane proteins in cancer progression and EMT. Eur J Cell Biol. 2022;101(2):151220.
11. Xie T, Fu D, Li K, Guo J, Xiao Z, Li Z, et al. Identification of a basement membrane gene signature for predicting prognosis and estimating the tumor immune microenvironment in prostate cancer. Aging (Albany NY). 2024;16(2):1581–604.
12. Li Y, Xu K, Zhang Y, Mao H, Qiu Q, Yan Z et al. Identification of a basement membrane-related genes signature with immune correlation in bladder urothelial carcinoma and verification in vitro. BMC Cancer. 2023;23(1).
13. Zhou F, Liu Y, Liu D, Xie Y, Zhou X. Identification of basement membrane-related signatures for estimating prognosis, immune infiltration

landscape and drug candidates in pancreatic adenocarcinoma. J Cancer. 2024;15(2):401–17.
14. Naka T, Boltze C, Kuester D, Samii A, Herold C, Ostertag H, et al. Intralesional fibrous septum in Chordoma: a clinicopathologic and immunohistochemical study of 122 lesions. Am J Clin Pathol. 2005;124(2):288–94.
15. Glentis A, Oertle P, Mariani P, Chikina A, El MF, Attieh Y, et al. Cancer-associated fibroblasts induce metalloprotease-independent cancer cell invasion of the basement membrane. Nat Commun. 2017;8(1):924.
16. Zhang T, Xia C, Zheng B, Hu H, Jiang L, Escobar D, et al. Integrating single-cell and Spatial transcriptomics reveals Endoplasmic reticulum stress-related CAF subpopulations associated with Chordoma progression. Neuro Oncol. 2024;26(2):295–308.
17. Bai J, Shi J, Zhang Y, Li C, Xiong Y, Koka H, et al. Gene expression profiling identifies two Chordoma subtypes associated with distinct molecular mechanisms and clinical outcomes. Clin Cancer Res. 2023;29(1):261–70.
18. Tibshirani R. The Lasso method for variable selection in the Cox model. Stat Med. 1997;16(4):385–95.
19. Ritchie ME, Phipson B, Wu D, Hu Y, Law CW, Shi W, et al. Limma powers differential expression analyses for RNA-sequencing and microarray studies. Nucleic Acids Res. 2015;43(7):e47.
20. Wilkerson MD, Hayes DN. ConsensusClusterPlus: a class discovery tool with confidence assessments and item tracking. Bioinformatics. 2010;26(12):1572–3.
21. Ashburner M, Ball CA, Blake JA, Botstein D, Butler H, Cherry JM, et al. Gene ontology: tool for the unification of biology. The gene ontology consortium. Nat Genet. 2000;25(1):25–9.
22. Kanehisa M, Furumichi M, Tanabe M, Sato Y, Morishima K. KEGG: new perspectives on genomes, pathways, diseases and drugs. Nucleic Acids Res. 2017;45(D1):D353–61.
23. Subramanian A, Tamayo P, Mootha VK, Mukherjee S, Ebert BL, Gillette MA, et al. Gene set enrichment analysis: a knowledge-based approach for interpreting genome-wide expression profiles. Proc Natl Acad Sci U S A. 2005;102(43):15545–50.
24. Friedman J, Hastie T, Tibshirani R. Regularization paths for generalized linear models via coordinate descent. J Stat Softw. 2010;33(1):1–22.
25. Yoshihara K, Shahmoradgoli M, Martinez E, Vegesna R, Kim H, Torres-Garcia W, et al. Inferring tumour purity and stromal and immune cell admixture from expression data. Nat Commun. 2013;4:2612.
26. Maeser D, Gruener RF, Huang RS. OncoPredict: an R package for predicting in vivo or cancer patient drug response and biomarkers from cell line screening data. Brief Bioinform. 2021;22(6).
27. Sharma A, Seow J, Dutertre CA, Pai R, Bleriot C, Mishra A, et al. Onco-fetal reprogramming of endothelial cells drives immunosuppressive macrophages in hepatocellular carcinoma. Cell. 2020;183(2):377–e39421.
28. McShane LM, Altman DG, Sauerbrei W, Taube SE, Gion M, Clark GM. REporting recommendations for tumor marker prognostic studies (REMARK). Breast Cancer Res Treat. 2006;100(2):229–35.
29. Cooper J, Giancotti FG. Integrin signaling in cancer: mechanotransduction, stemness, epithelial plasticity, and therapeutic resistance. Cancer Cell. 2019;35(3):347–67.
30. Sun F, Wang J, Sun Q, Li F, Gao H, Xu L, et al. Interleukin-8 promotes integrin beta3 upregulation and cell invasion through PI3K/Akt pathway in hepatocellular carcinoma. J Exp Clin Cancer Res. 2019;38(1):449.
31. Li F, Xu T, Chen P, Sun R, Li C, Zhao X, et al. Platelet-derived extracellular vesicles inhibit ferroptosis and promote distant metastasis of nasopharyngeal carcinoma by upregulating ITGB3. Int J Biol Sci. 2022;18(15):5858–72.
32. Cheng C, Liu D, Liu Z, Li M, Wang Y, Sun B, et al. Positive feedback regulation of LncRNA TPT1-AS1 and ITGB3 promotes cell growth and metastasis in pancreatic cancer. Cancer Sci. 2022;113(9):2986–3001.
33. Guo W, Cai Y, Liu X, Ji Y, Zhang C, Wang L, et al. Single-Exosome profiling identifies ITGB3 + and ITGAM + Exosome subpopulations as promising early diagnostic biomarkers and therapeutic targets for colorectal cancer. Res (Wash D C). 2023;6:0041.
34. Awwad K, Hu J, Shi L, Mangels N, Abdel MR, Zippel N, et al. Role of secreted modular calcium-binding protein 1 (SMOC1) in transforming growth factor beta signalling and angiogenesis. Cardiovasc Res. 2015;106(2):284–94.
35. Gersdorff N, Muller M, Schall A, Miosge N. Secreted modular calcium-binding protein-1 localization during mouse embryogenesis. Histochem Cell Biol. 2006;126(6):705–12.
36. Klemencic M, Novinec M, Maier S, Hartmann U, Lenarcic B. The heparin-binding activity of secreted modular calcium-binding protein 1 (SMOC-1) modulates its cell adhesion properties. PLoS ONE. 2013;8(2):e56839.
37. Wang J, Xia S, Zhao J, Gong C, Xi Q, Sun W. Prognostic potential of secreted modular Calcium-Binding protein 1 in Low-Grade glioma. Front Mol Biosci. 2021;8:666623.
38. Hayano Y, Sasaki K, Ohmura N, Takemoto M, Maeda Y, Yamashita T, et al. Netrin-4 regulates thalamocortical axon branching in an activity-dependent fashion. Proc Natl Acad Sci U S A. 2014;111(42):15226–31.
39. Moore SW, Tessier-Lavigne M, Kennedy TE. Netrins and their receptors. Adv Exp Med Biol. 2007;621:17–31.
40. Guenebeaud C, Goldschneider D, Castets M, Guix C, Chazot G, Delloye-Bourgeois C, et al. The dependence receptor UNC5H2/B triggers apoptosis via PP2A-mediated dephosphorylation of DAP kinase. Mol Cell. 2010;40(6):863–76.
41. Okazaki S, Ishikawa T, Iida S, Ishiguro M, Kobayashi H, Higuchi T, et al. Clinical significance of UNC5B expression in colorectal cancer. Int J Oncol. 2012;40(1):209–16.
42. Wu S, Guo X, Zhou J, Zhu X, Chen H, Zhang K, et al. High expression of UNC5B enhances tumor proliferation, increases metastasis, and worsens prognosis in breast cancer. Aging. 2020;12(17):17079–98.
43. Liu J, Zhang Z, Li ZH, Kong CZ. Clinical significance of UNC5B expression in bladder cancer. Tumour Biol. 2013;34(4):2099–108.
44. Shoulders MD, Raines RT. Collagen structure and stability. Annu Rev Biochem. 2009;78:929–58.
45. Li X, Wu WK, Xing R, Wong SH, Liu Y, Fang X, et al. Distinct subtypes of gastric cancer defined by molecular characterization include novel mutational signatures with prognostic capability. Cancer Res. 2016;76(7):1724–32.
46. Jiang Y, Chen F, Ren X, Yang Y, Luo J, Yuan J, et al. RNA-Binding protein COL14A1, TNS1, NUSAP1 and YWHAE are valid biomarkers to predict peritoneal metastasis in gastric cancer. Front Oncol. 2022;12:830688.
47. Miyake M, Hori S, Morizawa Y, Tatsumi Y, Toritsuka M, Ohnishi S, et al. Collagen type IV alpha 1 (COL4A1) and collagen type XIII alpha 1 (COL13A1) produced in cancer cells promote tumor budding at the invasion front in human urothelial carcinoma of the bladder. Oncotarget. 2017;8(22):36099–114.
48. Khalili AA, Ahmad MR. A review of cell adhesion studies for biomedical and biological applications. Int J Mol Sci. 2015;16(8):18149–84.
49. Glaviano A, Foo A, Lam HY, Yap K, Jacot W, Jones RH, et al. PI3K/AKT/mTOR signaling transduction pathway and targeted therapies in cancer. Mol Cancer. 2023;22(1):138.
50. Jaskiewicz A, Pajak B, Orzechowski A. The many faces of Rap1 GTPase. Int J Mol Sci. 2018;19(10).
51. Zhou Y, Xu J, Luo H, Meng X, Chen M, Zhu D. Wnt signaling pathway in cancer immunotherapy. Cancer Lett. 2022;525:84–96.
52. Hinshaw DC, Shevde LA. The tumor microenvironment innately modulates cancer progression. Cancer Res. 2019;79(18):4557–66.
53. Biffi G, Tuveson DA. Diversity and biology of Cancer-Associated fibroblasts. Physiol Rev. 2021;101(1):147–76.

Publisher's note

Springer Nature remains neutral with regard to jurisdictional claims in published maps and institutional affiliations.